Folding of a heterogeneous #-hairpin peptide from temperature-jump 2D IR spectroscopy

Citation: Jones, K. C., C. S. Peng, and A. Tokmakoff. "Folding of a heterogeneous -hairpin peptide from temperature-jump 2D IR spectroscopy." Proceedings of the National Academy of Sciences 110, no. 8 (February 19, 2013): 2828-2833.

As Published: http://dx.doi.org/10.1073/pnas.1211968110

Publisher: National Academy of Sciences (U.S.)

Persistent URL: http://hdl.handle.net/1721.1/80379

Version: Final published version: final published article, as it appeared in a journal, conference proceedings, or other formally published context

Folding of a heterogeneous β-hairpin peptide from temperature-jump 2D IR spectroscopy

Kevin C. Jones, Chunte Sam Peng, and Andrei Tokmakoff[1]

Department of Chemistry, Massachusetts Institute of Technology, Cambridge, MA 02139

Edited by Michael D. Fayer, Stanford University, Stanford, CA, and approved January 7, 2013 (received for review July 13, 2012)

We provide a time- and structure-resolved characterization of the folding of the heterogeneous β-hairpin peptide Tryptophan Zipper 2 (Trpzip2) using 2D IR spectroscopy. The amide I′ vibrations of three Trpzip2 isotopologues are used as a local probe of the midstrand contacts, β-turn, and overall β-sheet content. Our experiments distinguish between a folded state with a type I′ β-turn and a misfolded state with a bulged turn, providing evidence for distinct conformations of the peptide backbone. Transient 2D IR spectroscopy at 45 °C following a laser temperature jump tracks the nanosecond and microsecond kinetics of unfolding and the exchange between conformers. Hydrogen bonds to the peptide backbone are loosened rapidly compared with the 5-ns temperature jump. Subsequently, all relaxation kinetics are characterized by an observed 1.2 ± 0.2-μs exponential. Our time-dependent 2D IR spectra are explained in terms of folding of either native or nonnative contacts from a common compact disordered state. Conversion from the disordered state to the folded state is consistent with a zip-out folding mechanism.

protein folding | time-resolved spectroscopy | multidimensional | ultrafast

Even with technical advances in protein folding simulations and experiments, it remains difficult to compare them at a molecular level. As a result, the pictures that emerge from these studies differ. Experiments are commonly interpreted using two or three states separated along a reaction coordinate by transition states that are difficult to interpret. Molecular dynamics (MD) simulations provide richly detailed information on the conformational dynamics, often involving more configurational states than can be resolved in experiments (1–3). These heterogeneous folding scenarios reinforce funnel pictures of the folding to a native state (4). Although the connection between these pictures has been articulated (2), experimental validation of these concepts is scarce (5–7).

Bridging the gap between theory and experiment requires experiments that are both sensitive to different conformational states of a protein and have time resolution to characterize their interconversion. Toward this goal, we have studied the folding of the β-hairpin peptide Tryptophan Zipper 2 (Trpzip2, TZ2) using 2D IR spectroscopy. Our experiments probe the amide I′ vibration, which is primarily C = O stretching of the peptide backbone. By spectroscopically isolating peptide units through isotope labeling, they become reporters of hydrogen bonding (H-bonding) to the amide oxygen. To connect amide I′ spectral observations with structures from MD simulations, models of amide I′ IR spectroscopy have recently become available (8). With these tools, we have identified multiple conformations for TZ2 (9, 10), including at least two turn structures. Transient 2D IR (t-2D IR) spectroscopy of peptides has proven powerful for following peptide conformational dynamics (5, 11–13). Here, t-2D IR spectroscopy of three TZ2 isotopologues is used to follow the conformational changes induced by a fast temperature jump (T-jump) (12, 14).

TZ2 (Fig. 1) is a 12-residue peptide designed to form a type I′ β-turn due to stabilization by cross-strand H-bonds and packing of two pairs of tryptophan (Trp) indole rings (15). TZ2's small size and fast folding rates have made it an attractive system to study both experimentally (9, 10, 15–23) and computationally (3, 16, 18, 24–27), which has fostered comparison and enriched interpretation of results. In general, recent work has focused on discriminating between two folding processes: (*i*) hydrophobic collapse (25, 28), in which H-bond contacts are formed after hydrophobic contacts create a favorable collapsed state, and (*ii*) zipping (18, 26, 29), where native H-bonds (nHBs) form rapidly following a nucleation event. Although there is little consensus on structures, many recent simulations identified multiple stable states: native, disordered, misfolded, and partially folded (13, 24, 26, 27). When characterized, the folding transition state is usually identified as containing the inner turn H-bonds (25, 27). If the cross-strand H-bonds form sequentially, the peptide may fold through a zip-out (turn-to-termini) or zip-in mechanism, both of which have been observed in simulations (18, 26, 27, 29).

Early experiments interpreted a sigmoidal melting curve (15) and single exponential folding kinetics (18) as signs of two-state folding. However, recent experiments interpreted probe-dependent melting points measured with circular dichroism, fluorescence, FTIR, and 2D IR as signs of multistate behavior (10, 16, 20). Heterogeneous folding was also proposed based on frequency-dependent differences in isotope-labeled 2D IR experiments and rates in T-jump measurements (10, 17, 19, 21, 22). Despite many studies, there has been no consensus on the folding mechanism or the specific assignment of states. Both cross-strand H-bond formation and Trp packing are recognized as being important, but their relationship is unclear. Our results provide direct experimental evidence of heterogeneous folding of TZ2, which validates insights from MD simulations and indicates that classification of the folding mechanism purely by zipping or hydrophobic collapse oversimplifies the process.

Results

Equilibrium 2D IR Spectroscopy. In addition to the unlabeled (UL) TZ2 peptide, we studied two isotopomers labeled at the sites highlighted in Fig. 1. A ^{13}C label at the lysine isotope label (K8) carbonyl provides a reporter for the presence of H-bond 2 (Fig. 1) in the turn, whereas a dual threonine ^{13}C isotope label at the T3 and T10 carbonyl (TT) senses vibrational couplings due to contacts in the central region of the strands. Spectra for these peptides are shown in Fig. 2. UL TZ2 spectra show two distinct features of antiparallel β-sheets; the 1,635 cm^{-1} and weaker 1,670 cm^{-1} peaks are due to the $\nu_\perp$ and $\nu_\parallel$ modes, two delocalized vibrational modes that differ by the phase of vibration between adjacent amide units (9). In 2D IR spectra, the vibrational excitation frequency (ω_1) is correlated with a detection frequency (ω_3). Each resonance is a doublet composed of a positive peak (Fig. 2; fundamental, red) and negative peak (Fig. 2; overtone, blue) displaced to lower ω_3. The $\nu_\perp$ and $\nu_\parallel$ peaks have cross-peaks in Fig. 2 (*Upper Left*; weak positive ridge along ω_3 = 1,682 cm^{-1}) and in Fig. 2 (*Lower Right*; negative ridge along ω_3 = 1,625 cm^{-1}). The isotope-labeled C = O peaks in Fig. 2

Author contributions: K.C.J. and A.T. designed research; K.C.J. and C.S.P. performed research; K.C.J. analyzed data; and K.C.J., C.S.P., and A.T. wrote the paper.

The authors declare no conflict of interest.

This article is a PNAS Direct Submission.

[1]To whom correspondence should be addressed. E-mail: tokmakof@mit.edu.

This article contains supporting information online at www.pnas.org/lookup/suppl/doi:10.1073/pnas.1211968110/-/DCSupplemental.

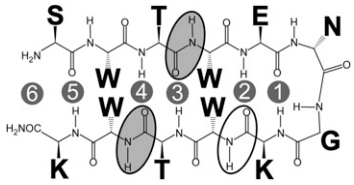

Fig. 1. Structure of TZ2 showing cross-strand H-bonds. The white and gray ovals depict isotope-labeled amide units for the K8 and TT isotopologues, respectively.

appear along the diagonal in the 1,575- to 1,620-cm^{-1} region. For the dual-label TT, there is a single diagonally elongated shoulder at 1,610 cm^{-1} (Fig. 2), whose large red shift relative to the single-label case is due to cross-strand amide couplings between the two threonine amide groups (10). Despite being a single label, the K8 spectrum displays two peaks separated by ~15 cm^{-1} (Fig. 2).

To make connections between structural and spectral features, the 2D IR spectra of varying conformational states obtained from Markov state analysis of MD simulations (3) were previously simulated using a model for the amide I′ vibrations (10, 30). To highlight the key features, four chosen conformational states are shown in Fig. 3 and a detailed description is found in the study by Smith et al. (10). The folded state corresponds to the native fold with an NMR-observed type I′ β-turn in which the K8, T3, and T10 oscillators are H-bonded to the opposite strand (15). The frayed state retains the native turn, except the N and C termini are frayed and the T3 and T10 contacts are slightly loosened. The bulged state retains central cross-strand contacts but has an unstructured turn and misregistered H-bonds that leave the oxygen of K8 solvent-exposed. The disordered state contains a variety of compact conformations that lack β-sheet structure. The experimental UL spectrum shares features with calculated spectra for the folded, bulged, and frayed conformers. The 1,610-cm^{-1} peak in the TT spectrum is reproduced in the folded and bulged simulated spectra. Disordering of the midstrand TT H-bonds causes the TT shoulder to shift to higher frequency (blue shift) and decrease in amplitude, as is shown in the bulged and frayed states and in the drop in intensity in the disordered spectrum (10).

The two K8 peaks are attributed to two turn conformations whose frequencies differ based on the number of H-bonds made to the labeled C = O (10, 31). The higher frequency (K8-2) peak at ω_1 = 1,610 cm^{-1} is assigned to the type I′ β-turn, in which TZ2 forms an H-bond across the turn to the N-H of E5, as is consistent with the folded and frayed simulated spectra. In a comparison of the bulged spectrum (Fig. 3), the lower frequency (K8-1) peak at ω_1 = 1,592 cm^{-1} is attributed to conformers in which the K8 carbonyl is solvent-exposed and can accept two H-bonds from water. It does not arise from an unfolded or disordered state, because 2D NMR restraints under similar conditions described a well-folded structure (15). Although the presence of two amide I peaks may also be seen in the case of multiple solvation states (32), water-solvated carbonyls have considerably broader line widths than observed for K8-2. Instead, this sharp line shape is consistent with the restricted, buried nature of the K8 oscillator in the folded state: one unique H-bonding configuration. Based on this reasoning and computational modeling, the presence of two peaks is evidence of conformational heterogeneity.

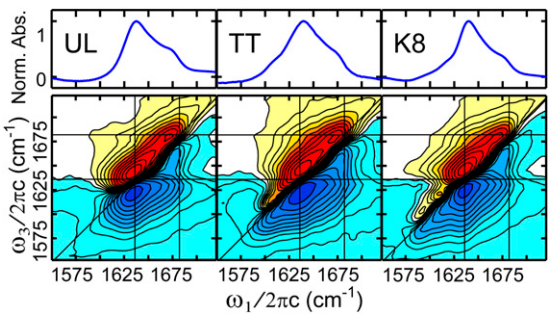

Fig. 2. Equilibrium 35 °C 2D IR surfaces with parallel (ZZZZ) acquisition polarization and τ_2 = 150 fs. Red contours refer to positive amplitude, and blue contours refer to negative amplitude. The 2D IR spectra are individually normalized to the maximum of the absolute value and scaled such that 25 linearly spaced contours span the entire magnitude range of $\sinh^{-1}(S_{Norm.} \times 27.29)$. Norm. Abs., normalized absorbance.

Previous equilibrium experiments have also identified the temperature-dependent spectral changes expected for TZ2 and alanine substitutes (TZ2C) (9, 10, 15, 20). On heating, the UL β-sheet peaks decrease and broaden concomitant with the increase of intensity at 1,660 cm^{-1}, spectral changes that can be assigned to full disordering or partial fraying of the structure, which leaves residual β-turns (9, 10). Broadening and blue-shifting of peaks were also observed and are expected based on the general amide I′ response to temperature (23, 33). Although both K8 turn configurations are lost with increasing temperature due to net conversion to a disordered or partially disordered state, the native type I′ β-turn configuration (K8-2) is retained at a higher population relative to the bulged turn population (K8-1) (10).

T-Jump Spectroscopy. We performed T-jump infrared experiments using the methods described by Jones et al. (23). The initial sample temperature was T_i = 35 °C, and it was jumped 10 °C in 5 ns. Conformational changes induced by the T-jump were followed with t-2D IR, transient dispersed pump–probe (t-DPP), and transient absorption (t-A) experiments. Whereas t-A is a traditional measure of the change in linear absorbance, t-2D IR and t-DPP measure the change in a nonlinear signal. The t-DPP spectrum is equal to the projection of the t-2D IR spectrum onto the ω_3 detection axis, but because it is acquired in one frequency dimension, it can be sampled more rapidly. We present the spectral results from the t-2D IR and the time dependence from the corresponding t-DPP. t-A results, raw t-DPP spectra (Fig. S1), and raw t-2D IR spectra (Fig. S2) are presented in *SI Text*.

As shown in Fig. 4, characteristic time traces from the t-DPP data exhibit three general time scales: a <5-ns response limited by the T-jump pulse width, a 1- to 2-μs response, and a 1-ms time scale reequilibration of the temperature as the heat diffuses out of the sample. These time scales are observed in all t-DPP and t-2D IR spectra, with varying amplitudes. Although exponential fits of the t-DPP traces range from 1.0–2.0 μs (Table S1), within their 95% confidence intervals, all isotope label variants can be described by a 1.2-μs relaxation time. This is consistent with previously measured relaxation times (19). The time scales indicate that our observations arise from activated kinetics of exchange between states on the microsecond time scale, and from diffusion-limited relaxation within these states following the T-jump on picosecond-to-nanosecond time scales.

To analyze the time-dependent spectral changes in the T-jump t-DPP and t-2D IR experiments, we applied a singular value decomposition (SVD) analysis to their spectra (*SI Text* and Figs. S3–S6). SVD linearly decomposes the data into spectra that share a common time dependence. Our analysis encapsulates the spectral changes in the t-DPP and t-2D IR experiments that occur during the nanosecond period and the subsequent microsecond period through two spectra, S_n and S_μ, respectively, and their time-varying amplitudes, P_n and P_μ. The nanosecond and microsecond spectral components are shown in Fig. 5 *B* and *C*, along with their matching t-DPP time traces in Fig. 5*D*. The raw data are similar to the SVD components, and they are presented in Fig. S1. P_n traces immediately jump to a positive value following the T-jump, whereas P_μ

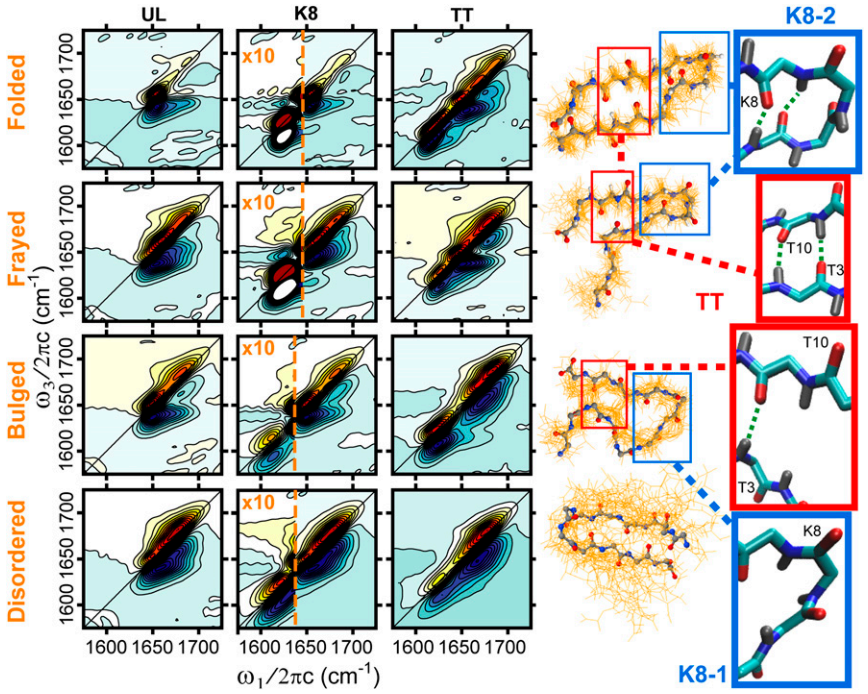

Fig. 3. Two-dimensional IR spectra of TZ2 isotopologues simulated from select Markov states. Spectra are for $\tau_2 = 0$ fs and are plotted with linear contours. On the right, characteristic structures for each state are shown. Adapted with permission from [Smith AW, Lessing J, Ganim Z, Peng SC, Tokmakoff A, Roy S, Jansen TLC, Knoester J (2010) *J Phys Chem B* 114(34):10913–10924]. Copyright 2010 American Chemical Society. Structures are derived from 425 K MD simulations (3, 24) that were dominated by disordered configurations (89%). The folded (8%), misregistered (similar to bulged, 2%), and frayed (0.1%) states were present in much lower populations. MD simulations were only used to sample representative structures for spectral simulations, and they are not a reflection of the conclusions of this work.

traces grow in on a 1.2 (±0.2)-μs exponential time scale. Both return to equilibrium concomitant with the temperature reequilibration.

t-2D IR. ***Nanosecond response.*** For t-2D IR difference spectra, the sign of gain and loss features depends on the sign of the equilibrium peak (34) (Fig. S7). Generally, because a diagonal peak in the equilibrium spectrum is positive (red) above and negative (blue) below the diagonal, loss of that peak in the difference spectrum shows up as blue above and red below the diagonal. The UL S_n spectrum has two sets of paired features: loss along the diagonal maximized on the low-frequency side of equilibrium peaks and gain in the off-diagonal regions (marked by pink arrows in Fig. 5*B*). These changes are consistent with a blue shift and a transition from inhomogeneous to homogeneously broadened peaks (23) (Fig. S7). This suggests the T-jump induces increased conformational fluctuations (exhibited by broadening) and a net weakening of peptide/peptide and/or peptide/water H-bonds (exhibited by blue shifting).

Thermal fluctuations, loss or weakening of H-bonding surrounding the TT and K8 oscillators, and weakening of TT cross-strand couplings are observed in TT and K8 S_n spectra as loss on the red side of the equilibrium peaks for the TT and K8-1 (green arrows in Fig. 5*B*). The blue shifting of the TT peak is subtle due to overlap with diagonal loss features, but it is apparent through off-diagonal growth (pink arrow in Fig. 5*B*) and a dip in the negative intensity (white arrow in Fig. 5*B*). The K8-2 peak shows gain on the high-frequency side of the resonance (white arrow in Fig. 5*B*) and loss on the low-frequency side, which could be due to weakening of the H-bond to the K8-2 configuration. Alternatively, a solvent-exposed K8-1 oscillator could lose H-bonds to the solvent, shifting it up in frequency so that it might overlap with K8-2. In either case, fast changes in H-bond strength or number without significant peptide conformational change are involved, and the TT and K8-2 responses indicate that the midstrand and turn-region H-bonds remain intact on the nanosecond time scale.

Microsecond response. The S_μ spectra in Fig. 5*C* highlight the spectral changes that occur exclusively on the microsecond time scale, and they display signatures of significant conformational changes. Along the diagonal of the UL spectrum, loss of peaks at 1,640 cm^{-1} ($\nu_\perp$) and 1,680 cm^{-1} ($\nu_\parallel$) indicates disruptions to the antiparallel β-sheet (10, 13). In the 1,660-cm^{-1} region, there is a concomitant increase of a broad doublet peak (pink arrows in Fig. 5*C*), which we assign to the appearance of disordered structures (10). Such spectral changes are consistent with fraying of the termini or complete unfolding of the turn.

The TT and K8 isotope-region S_μ spectra display loss along the diagonal consistent with the equilibrium spectrum but show no noticeable gain features. Loss of the TT and K8-2 peaks indicates that the midstrand and turn region H-bonds are broken on the microsecond time scale. The K8-1 peak is also lost in S_μ, indicating loss of misfolded conformations in which the K8 carbonyl is pointing out into the solvent. The microsecond time scale associated with loss of these misfolded K8-1 configurations indicates a significant barrier separating the misfolded configurations from the disordered state.

Discussion

Based on our experiments and prior characterization of this system, we propose an energy landscape for the folding of TZ2 in Fig. 6. Although the observation of only one interwell exponential relaxation time scale (~1.2 μs) generally implies two states, our

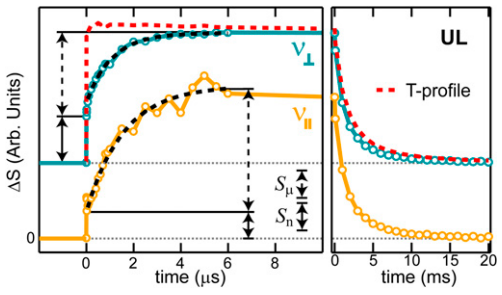

Fig. 4. Normalized traces from the t-DPP data of TZ2 UL shown in Fig. S1 illustrating the nanosecond and microsecond time scales observed in the data at $\nu_\perp$ = 1,640 cm^{-1} and $\nu_\parallel$ = 1,670 cm^{-1}. The dashed red curve indicates the temperature profile. The solid and dashed vertical arrows indicate the ratio of S_n and S_μ amplitude for these frequencies, which are offset for clarity. Arb., arbitrary.

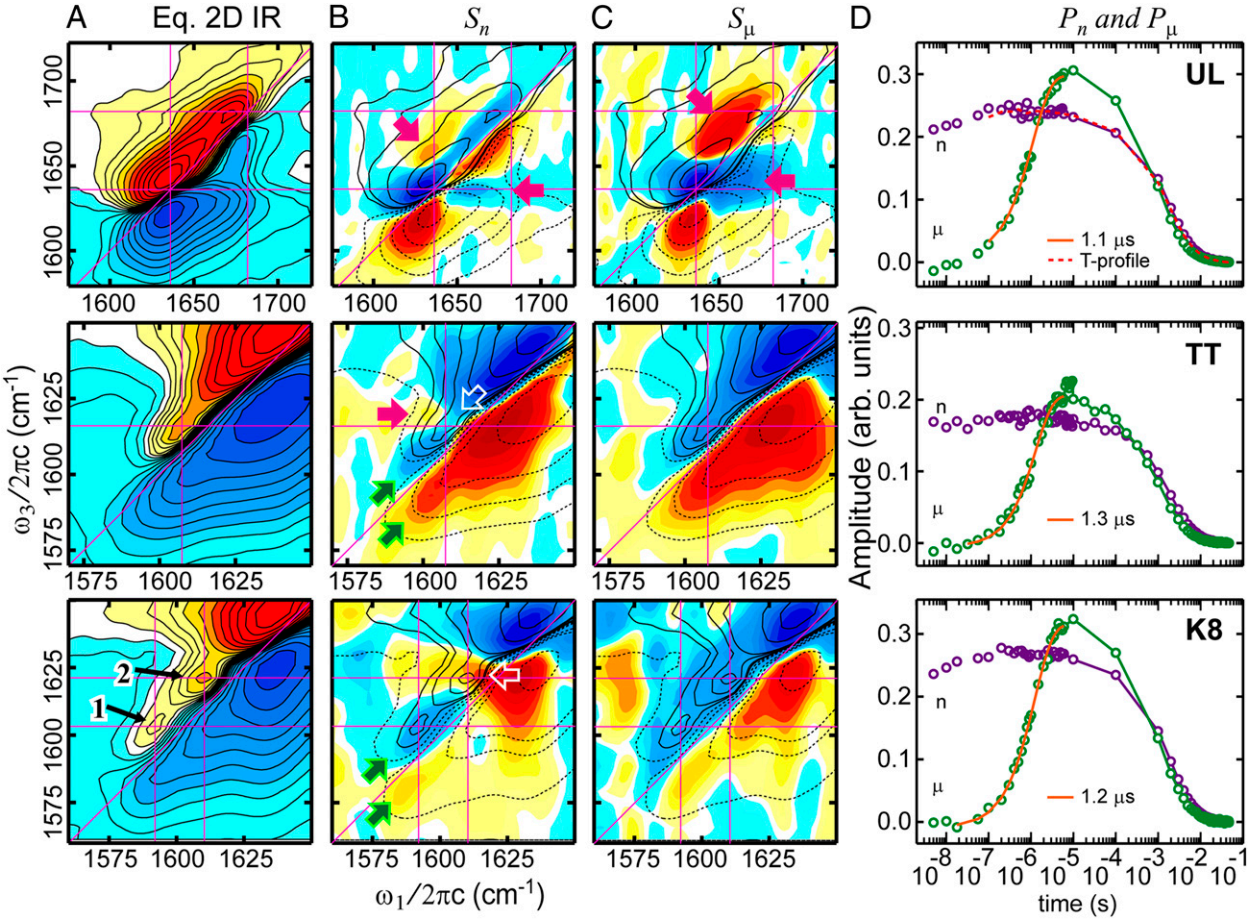

Fig. 5. Two-dimensional IR data (*A–C*) and t-DPP (*D*) at τ_2 = 150 fs for TZ2 UL (*Top*), TT (*Middle*), and K8 (*Bottom*) following T-jump. (*A*) Equilibrium 2D IR spectra highlight the isotope-labeled region for TT and K8. (*B* and *C*) t-2D IR basis spectra (raw data shown in Fig. S2) describe the spectral changes on nanosecond and microsecond time scales. Red corresponds to a positive difference of spectral amplitude, and blue represents a negative difference. Loss of diagonal peaks is observed as blue above and red below the diagonal. Contours from the equilibrium spectra are shown overlaying the transient spectra. Contours and shading in *A–C* are drawn as described in Fig. 2. (*D*) Time-dependent amplitude changes for the t-2D IR spectra shown in *B* and *C*, obtained from SVD analysis of t-DPP spectra in Fig. S1.

spectral assignments lead us to identify three thermodynamically distinct states: folded (*F*), misfolded (*M*), and disordered (*D*). Within the folded and misfolded wells, we also identify a change in the average structures between the initial (F_0, M_0) and final (F, M) temperatures spanned by the T-jump. The surfaces represent hypothetical potentials of mean force along representative coordinates: the nHB number, non-nHB number, type I′ β-turn folding (turn rmsd), and extent of disorder and solvation of the backbone [radius of gyration (R_g)].

The states are characterized as follows using the H-bond numbering convention in Fig. 1.

Folded. Folded (F and F_0) states contain the type I′ β-turn, H-bonds 1–4 (and perhaps H-bond 5), and Trp side-chain packing presented in the NMR structure and in the folded state configuration from simulations. The F_0 spectrum contains $\nu_\perp$ and $\nu\|$ peaks, the K8-2 peak, and a red-shifted TT peak. On thermal excitation, the F state may include frayed configurations with H-bonds 1–3 and loosened packing of Trp2/Trp11. Relative to F_0, the F spectrum shows blue-shifted K8-2 and TT frequencies.

Misfolded. Misfolded (M and M_0) states exhibit solvent-exposed K8 carbonyls with bulged turns, misregistration of β-strands, some non-nHBs near the termini, and reduced Trp packing. These spectra feature the K8-1 peak, which is expected to blue-shift on thermal excitation.

Disordered. Disordered (*D*) states are unstructured states. The structures vary from compact to extended, which is observed as a wide distribution in the R_g in Fig. 6. Configurations also vary in the solvent exposure of K8. The *D* spectrum contains a single disordered main amide I′ peak at ~1,660 cm^{-1}, and the TT and K8 peaks are expected to be weak and broad, spanning the entire 1,580- to 1,610-cm^{-1} range.

The equilibrium ensemble has a high fraction of folded structures with native type I′ β-turns. The UL spectrum indicates antiparallel contacts between strands, and the TT and K8-2 peaks indicate H-bonds 2–4 are intact in these equilibrium β-turn conformations. The geometrical constraints imposed by H-bonds 2–4 indicate that an intact H-bond 1 is highly probable in the folded conformation. Previous dual labeling of mutant TZ2C has shown that the A1 and A10 residues are not coupled, indicating fraying at the end (19). Thus, we estimate that the free energy minimum of F_0 lies at four cross-strand nHBs.

For species starting in the folded well (F_0) at T_i, the T-jump induces an abrupt <5-ns relaxation to F with minor conformational changes, leading to blue shifts of the K8-2 and TT peaks (white arrows in Fig. 5*B*). This suggests loosening of the cross-strand nHBs, but the signs of complete loss of these H-bonds are not

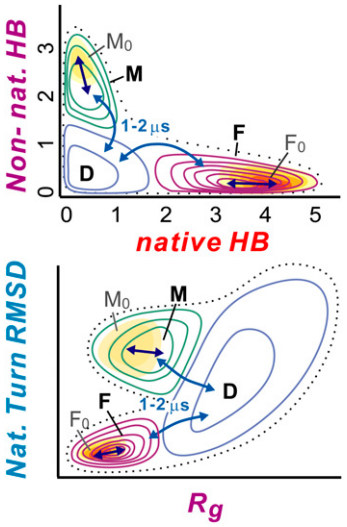

Fig. 6. Experimentally informed proposal for the TZ2 conformational free energy surface displayed as a function of four coordinates. Different coordinates are used for each plot. Non-nHBs (Non-nat. HB) and nHBs (native HB) refer to the total number of cross-strand H-bonds (not the labels from Fig. 1). Native turn rmsd (Nat. Turn RMSD) describes the structure of the ENGK relative to the native type I′ β-turn. R_g describes the compactness of the full structure. Arrows indicate movement of the population on either the <5-ns (black) or 1- to 2-μs time scale (blue).

observed. Loss of H-bond 4 would result in similar spectral changes. These spectral changes suggest that the folded well at the final temperature (F) is slightly shifted to a lower nHB number from F_0, most likely as a result of fraying.

The presence of the K8-1 peak at 35 °C (Fig. 2) shows that stable conformations exist with solvent-exposed K8 carbonyls, the M_0 state. This peak intensity decreases with increasing temperature, indicating that it is distinct from the D state, whose population increases with temperature. Comparing the intensity ratio of the K8-2 and K8-1 peaks at T_i = 35 °C indicates that ∼70% of the population has native turn conformations and 30% has a solvent-exposed K8, assuming a negligible population of D. As with the β-turn structures, we expect the loss of H-bonds due to T-jump will cause a shift in the K8-1 frequency. The solvent-exposed K8 conformations are disturbed on the <5-ns time scale (Fig. 5*B*), and are reflected in the energy landscape as relaxation from M_0 to M.

The lack of growth in the K8-1 isotope label region (Fig. 5 *B* and *C*) suggests that the disordered state is not completely extended into the solvent, where multiple H-bonds can form to an exposed K8 carbonyl. We therefore represent the D state through a broad distribution of R_g, where the highest probability conformation is relatively compact. Consistent with this conclusion, the D state is also collapsed in many simulations (16, 18, 25, 27) and experiments (16, 17, 35). Based on melting curves, a minimal population (<5%) exists in disordered states (distinct from misfolded states) in this temperature range (9, 10, 15, 20).

On the ∼1.2-μs time scale, the loss of K8-2 (Fig. 5*C*) indicates conformational changes involving the unfolding of the type I′ β-turn and a transition from $F \rightarrow D$. The K8-1 (Fig. 5*C*) peak is lost on the same microsecond time scale as the K8-2 peak, indicating that T-jump–induced conformational changes to the solvent-exposed K8 structures proceed over a significant energetic barrier. Furthermore, because T-jump relaxation rates between two states are related to the forward and reverse rates, this process is connected to the change to K8-2 in some manner. It may appear that the synchronized loss of K8-1 and K8-2 peaks on the ∼1.2-μs time scale and exponential kinetics are consistent with two-state folding in which the K8-1 and K8-2 structures are both of a folded nature and exchange rapidly with <5-ns kinetics. Our conclusion of conformationally distinct F and M states is based on the spectral assignment of the K8-1 and K8-2 peaks to bulged and folded structures based on spectral simulations (10), line-width arguments, and multiple rates reported in separate experiments (19). The great conformational dissimilarity of misregistered structures relative to the native state indicates that direct transitions between F and M states are improbable. These states differ in strand orientation, H-bond registry, and global configuration of side chains. A concerted inversion of strands and side chains is needed to make this transition; therefore, an exchange of these structures is far more likely to proceed stepwise through the D state, as has been observed in simulations (3).

In the general case, T-jump relaxation kinetics involving three states in series would exhibit biexponential relaxation with time scales that depend on all forward and reverse rates. The amplitudes of the two exponential phases, however, depend on the individual rates and the changes in populations induced by the T-jump, such that it is not unusual for a single exponential to dominate the observed relaxation. Because the spectral assignments lead us to propose three states, we conclude that we are in the regime where the amplitude of the second exponential is negligible. This is consistent with experiments on the mutant TZ2C, which found frequency-dependent folding rates consistent with an intermediate but a convergence of relaxation time scales for temperatures >45 °C (19). We expect the fastest rates are for the $D \rightarrow M$ and $D \rightarrow F$ transitions, a reasonable assumption at this temperature. Based on the previously determined relative populations between D, M, and F (10) and the 1- to 2-μs observed relaxation rate, we can conclude that these rates fall in the 1- to 5-μs window and the corresponding unfolding rates are twofold to 10-fold slower. These rates are similar to those observed for other hairpins (12, 29, 36).

On the basis of these observations and the proposed energy landscape, it is possible to draw some conclusions regarding the mechanism of folding. The β-strand structure, midstrand H-bonds, and turn H-bond are lost simultaneously on the microsecond time scale, but the observation that H-bonds 5–6 are already frayed suggests a zip-out mechanism for the $D \rightarrow F$ transition. The transition state for this process would have H-bonds 1 and/or 2 intact, indicating that turn nucleation would appear to be the rate-limiting step for $D \rightarrow F$ folding (29). This is consistent with simulations that identify a partially folded peptide with two to three H-bonds as a short-lived transition state (25, 27).

The proposed free energy surfaces in Fig. 6 can be compared with similar potentials of mean force calculated from simulations of β-hairpin folding (26, 27). Gao and coworkers (27) describe the transition from an extended state to a folded form through a partially folded state with possible excursions through a misfolded form, which bears similarity to our M. The *F-D-M* transition is much like the exchange of folded and misfolded conformers described in recent simulations of the protein G, B1 domain hairpin peptide GB1 (37, 38).

The compact nature of our disordered state indicates that it retains hydrophobic contacts, although the Trps are likely disordered. This is consistent with fluorescence experiments, which have noted that full loss of the hydrophobic collapsed structure only occurs under strongly denaturing conditions (16, 17). Although conducted under different conditions, T-jump fluorescence relaxation rates were also in the microsecond time range (17, 22). The coincidence of rates determined with IR (sensitive to H-bonding structure) and fluorescence (sensitive to Trp packing) indicates that Trp ordering and H-bonding are highly correlated. This is not surprising, because, geometrically, correct H-bonding and Trp packing for the $D \rightarrow F$ transition require nearly native contacts of side chains and the backbone. It is possible to conclude that some hydrophobic clustering will accompany both the $D \rightarrow M$ and $D \rightarrow F$ transitions. Thus, a simple description of the folding of TZ2 solely in terms of zipping or hydrophobic collapse does not seem appropriate.

Is the folding of this hairpin heterogeneous? Despite observing monoexponential kinetics, which we reconcile above, the structural assignments clearly indicate the presence of multiple conformers. Ultimately, conclusive evidence for heterogeneous folding requires conformer-specific experimental observables combined with clear evidence of exchange kinetics between these multiple states. Experimental observations of nonexponential kinetics (39) or probe-dependent kinetics (5, 12, 17) are suggestive but not definitive. One must associate such behavior with clearly resolved conformers, which 2D IR experiments are now able to do (10, 31). In the present case, the T-jump exchange processes are not well separated. As such, experiments that leave no question as to the presence of heterogeneous folding are still needed.

Conclusion

These studies illustrate how T-jump t-2D IR experiments in conjunction with isotope labeling can evaluate conformational variation in proteins and the manner in which these conformers interconvert. Furthermore, these experiments bridge the gap between experiment and atomistically detailed MD simulations. In the case of the peptide TZ2, we experimentally identify three distinct conformational ensembles: a folded state with four cross-strand H-bonds and a type I′ β-turn, a misfolded state with a bulged turn and misregistered contacts, and a disordered state that is unstructured and predominantly compact. Conversion between the misfolded and folded states requires loss of stabilizing native or nonnative contacts and proceeds most efficiently through the disordered state. The dominant population flux connects disordered and folded states in a manner consistent with the widely reported zipping mechanism. Overall, the perspective here argues that for this system, and likely others, a thermal unfolding process is not characterized by transitions from a single compact native conformation to a denatured state with randomized configurations of the backbone and side chains but, instead, represents a shifting of populations within a heterogeneous ensemble that contains conformational preferences and varying degrees of disorder.

Materials and Methods

This study integrates the development of T-jump t-2D IR spectroscopy with the extensive equilibrium characterization of the structural heterogeneity of TZ2. Many of these experimental details have been described in prior work and are also summarized in *SI Text*. Briefly, the solid-phase synthesis and characterization of TZ2 samples are discussed by Smith et al. (9). The design of the T-jump t-2D IR spectrometer (40), the processing of t-2D IR data (23), and heterodyne-detected dispersed vibrational echo spectroscopy (41), from which the t-DPP values are calculated, have been described previously. Each T-jump time series of t-2D IR spectra is analyzed with a protocol built on established SVD procedures described in detail in *SI Text*.

ACKNOWLEDGMENTS. Our understanding of TZ2 spectroscopy has benefited greatly from collaboration with Santanu Roy and Thomas L. C. Jansen. We also thank Carlos R. Baiz for comments on the manuscript. This work was supported by National Science Foundation Grants CHE-0616575 and CHE-0911107.

1. Noé F, Schütte C, Vanden-Eijnden E, Reich L, Weikl TR (2009) Constructing the equilibrium ensemble of folding pathways from short off-equilibrium simulations. *Proc Natl Acad Sci USA* 106(45):19011–19016.
2. Dill KA (1999) Polymer principles and protein folding. *Protein Sci* 8(6):1166–1180.
3. Chodera JD, Singhal N, Pande VS, Dill KA, Swope WC (2007) Automatic discovery of metastable states for the construction of Markov models of macromolecular conformational dynamics. *J Chem Phys* 126(15):155101.
4. Dill KA, Chan HS (1997) From Levinthal to pathways to funnels. *Nat Struct Biol* 4(1):10–19.
5. Ihalainen JA, et al. (2008) Alpha-Helix folding in the presence of structural constraints. *Proc Natl Acad Sci USA* 105(28):9588–9593.
6. Mello CC, Barrick D (2004) An experimentally determined protein folding energy landscape. *Proc Natl Acad Sci USA* 101(39):14102–14107.
7. Prigozhin MB, Gruebele M (2011) The fast and the slow: Folding and trapping of λ6-85. *J Am Chem Soc* 133(48):19338–19341.
8. Jansen TL, Knoester J (2006) A transferable electrostatic map for solvation effects on amide I vibrations and its application to linear and two-dimensional spectroscopy. *J Chem Phys* 124(4):044502.
9. Smith AW, Chung HS, Ganim Z, Tokmakoff A (2005) Residual native structure in a thermally denatured β-hairpin. *J Phys Chem B* 109(36):17025–17027.
10. Smith AW, et al. (2010) Melting of a beta-hairpin peptide using isotope-edited 2D IR spectroscopy and simulations. *J Phys Chem B* 114(34):10913–10924.
11. Kolano C, Helbing J, Kozinski M, Sander W, Hamm P (2006) Watching hydrogen-bond dynamics in a β-turn by transient two-dimensional infrared spectroscopy. *Nature* 444(7118):469–472.
12. Smith AW, Tokmakoff A (2007) Probing local structural events in β-hairpin unfolding with transient nonlinear infrared spectroscopy. *Angew Chem Int Ed Engl* 46(42):7984–7987.
13. Zhuang W, Cui RZ, Silva D-A, Huang X (2011) Simulating the T-jump-triggered unfolding dynamics of trpzip2 peptide and its time-resolved IR and two-dimensional IR signals using the Markov state model approach. *J Phys Chem B* 115(18):5415–5424.
14. Chung HS, Ganim Z, Jones KC, Tokmakoff A (2007) Transient 2D IR spectroscopy of ubiquitin unfolding dynamics. *Proc Natl Acad Sci USA* 104(36):14237–14242.
15. Cochran AG, Skelton NJ, Starovasnik MA (2001) Tryptophan zippers: Stable, monomeric β-hairpins. *Proc Natl Acad Sci USA* 98(10):5578–5583.
16. Yang WY, Pitera JW, Swope WC, Gruebele M (2004) Heterogeneous folding of the trpzip hairpin: Full atom simulation and experiment. *J Mol Biol* 336(1):241–251.
17. Yang WY, Gruebele M (2004) Detection-dependent kinetics as a probe of folding landscape microstructure. *J Am Chem Soc* 126(25):7758–7759.
18. Snow CD, et al. (2004) Trp zipper folding kinetics by molecular dynamics and temperature-jump spectroscopy. *Proc Natl Acad Sci USA* 101(12):4077–4082.
19. Hauser K, Krejtschi C, Huang R, Wu L, Keiderling TA (2008) Site-specific relaxation kinetics of a tryptophan zipper hairpin peptide using temperature-jump IR spectroscopy and isotopic labeling. *J Am Chem Soc* 130(10):2984–2992.
20. Huang R, et al. (2009) Cross-strand coupling and site-specific unfolding thermodynamics of a trpzip β-hairpin peptide using 13C isotopic labeling and IR spectroscopy. *J Phys Chem B* 113(16):5661–5674.
21. Hauser K, et al. (2010) Comparison of isotopic substitution methods for equilibrium and t-jump infrared studies of β-hairpin peptide conformation. *J Phys Chem B* 114(35):11628–11637.
22. Narayanan R, Pelakh L, Hagen SJ (2009) Solvent friction changes the folding pathway of the tryptophan zipper TZ2. *J Mol Biol* 390(3):538–546.
23. Jones KC, Ganim Z, Peng CS, Tokmakoff A (2012) Transient two-dimensional spectroscopy with linear absorption corrections applied to temperature-jump two-dimensional infrared. *J Opt Soc Am B* 29(1):118–129.
24. Pitera JW, Haque I, Swope WC (2006) Absence of reptation in the high-temperature folding of the trpzip2 β-hairpin peptide. *J Chem Phys* 124(14):141102.
25. Zhang J, Qin M, Wang W (2006) Folding mechanism of β-hairpins studied by replica exchange molecular simulations. *Proteins* 62(3):672–685.
26. Nymeyer H (2009) Energy landscape of the trpzip2 peptide. *J Phys Chem B* 113(24):8288–8295.
27. Yang L, Shao Q, Gao YQ (2009) Thermodynamics and folding pathways of trpzip2: An accelerated molecular dynamics simulation study. *J Phys Chem B* 113(3):803–808.
28. Dinner AR, Lazaridis T, Karplus M (1999) Understanding β-hairpin formation. *Proc Natl Acad Sci USA* 96(16):9068–9073.
29. Muñoz V, Thompson PA, Hofrichter J, Eaton WA (1997) Folding dynamics and mechanism of β-hairpin formation. *Nature* 390(6656):196–199.
30. Roy S, Jansen TLC, Knoester J (2010) Structural classification of the amide I sites of a β-hairpin with isotope label 2DIR spectroscopy. *Phys Chem Chem Phys* 12(32):9347–9357.
31. Backus EHG, et al. (2010) 2D-IR study of a photoswitchable isotope-labeled α-helix. *J Phys Chem B* 114(10):3735–3740.
32. Kwac K, Lee H, Cho M (2004) Non-Gaussian statistics of amide I mode frequency fluctuation of N-methylacetamide in methanol solution: Linear and nonlinear vibrational spectra. *J Chem Phys* 120(3):1477–1490.
33. Amunson KE, Kubelka J (2007) On the temperature dependence of amide I frequencies of peptides in solution. *J Phys Chem B* 111(33):9993–9998.
34. Bredenbeck J, et al. (2003) Transient 2D-IR spectroscopy: Snapshots of the nonequilibrium ensemble during the picosecond conformational transition of a small peptide. *J Phys Chem B* 107(33):8654–8660.
35. Dyer RB, et al. (2005) Hairpin folding dynamics: The cold-denatured state is predisposed for rapid refolding. *Biochemistry* 44(30):10406–10415.
36. Du D, Zhu Y, Huang C-Y, Gai F (2004) Understanding the key factors that control the rate of β-hairpin folding. *Proc Natl Acad Sci USA* 101(45):15915–15920.
37. Bonomi M, Branduardi D, Gervasio FL, Parrinello M (2008) The unfolded ensemble and folding mechanism of the C-terminal GB1 β-hairpin. *J Am Chem Soc* 130(42):13938–13944.
38. Best RB, Mittal J (2011) Microscopic events in β-hairpin folding from alternative unfolded ensembles. *Proc Natl Acad Sci USA* 108(27):11087–11092.
39. Volk M, et al. (1997) Peptide conformational dynamics and vibrational stark effects following photoinitiated disulfide cleavage. *J Phys Chem B* 101(42):8607–8616.
40. Chung HS, Khalil M, Smith AW, Tokmakoff A (2007) Transient two-dimensional IR spectrometer for probing nanosecond temperature-jump kinetics. *Rev Sci Instrum* 78(6):063101.
41. Jones KC, Ganim Z, Tokmakoff A (2009) Heterodyne-detected dispersed vibrational echo spectroscopy. *J Phys Chem A* 113(51):14060–14066.